Supporting Information

Atomically Dispersed Pd on ZrO_2 for Efficient Nitrite Electroreduction to Ammonia

Wenyu Du, Zeyi Sun, Chaofan Qiang, Kai Chen, Ke Chu*

School of Materials Science and Engineering, Lanzhou Jiaotong University, Lanzhou 730070, China.

*Corresponding author. chuk630@mail.lzjtu.cn (K. Chu)

Experimental section

7.40 g of $ZrO(NO_3)_2 \cdot xH_2O$ and 19.22 g of urea were dissolved in 80 mL of deionized water. And the mixed solution was transferred to a Teflon-lined stainless steel autoclave and kept under 160 ℃ for 20 h. After cooling, the precipitates were washed with deionized water several times and dried at 80 ℃ for 12 h. The dried precipitates were then calcined in a muffle furnace at 500 ℃ for 3 h to obtain ZrO_2. To prepare Pd_1/ZrO_2, an impregnation solution was used by dissolving 0.30 g of $PdCl_2$ in 30 mL of deionized water. The as-prepared ZrO_2 was then immersed in impregnation solution for 1 h, followed by drying under vacuum at 110 ℃ to obtain Pd_1/ZrO_2.

Electrochemical experiments

Electrochemical measurements were carried out on a CHI-760E electrochemical workstation using a three-electrode cell, with Ag/AgCl (saturated KCl), Pt foil and catalyst coated on carbon cloth (CC, 1 × 1 cm^2) as reference, counter and working electrodes, respectively. All potentials were referenced to reversible hydrogen electrode (RHE) in terms of E (V vs. RHE) = E (V vs. Ag/AgCl) + 0.198 V + 0.059 × pH. The CC substrate (1×1 cm^2) was pretreated by soaking it in 0.5 M H_2SO_4 for 12 h, and then washed with deionized water several times and dried at 60 ℃ for 24 h. The catalyst ink was prepared by dispersing 1 mg of the catalysts in 100 μL of ethyl alcohol containing 5 μL of Nafion (5 wt%) under ultrasonication. The catalyst inks were dropped onto CC (0.2 $mg \cdot cm^{-2}$) to form the working electrodes. The electrochemical NO_2RR measurements were performed 0.5 M Na_2SO_4 solution containing 0.1 M $NaNO_2$ using an H-type electrochemical cell separated by a Nafion 211 membrane. After each chronoamperometry test at certain potential for 1 h, the liquid products were analyzed by various colorimetric methods using UV-vis absorbance spectrophotometer (MAPADA P5), while the gas products (H_2, N_2) were analyzed by gas chromatography (Shimadzu GC2010).

Determination of NH_3

The generated NH_3 was determined by the indophenol blue method[1]. Typically, 0.5 mL of electrolyte was removed from the electrochemical reaction vessel and

diluted 50 times with deionized water. Then 2 mL of diluted solution was removed into a clean vessel followed by sequentially adding NaOH solution (2 mL, 1 M) containing $C_7H_6O_3$ (5 wt.%) and $C_6H_5Na_3O_7$ (5 wt.%), NaClO (1 mL, 0.05 M), and $Na_2Fe(CN)_5NO \cdot 2H_2O$ (0.2 mL, 1wt.%) aqueous solution. After the incubation for 2 h at room temperature, the mixed solution was subjected to UV-vis measurement using the absorbance at 655 nm wavelength. The concentration-absorbance curves were calibrated by the standard NH_4Cl solution with a series of concentrations[2, 3].

Calculations of NH_3 yield rate and NH_3-Faradaic efficiency

$$NH_3\ yield\ rate\ (\mu \cdot h^{-1} \cdot mg_{cat}^{-1}) = \frac{C_{NH3} \times V}{t \times A} \quad (1)$$

$$NH_3 - Faradaic\ efficiency(\%) = \frac{6 \times F \times C_{NH3} \times V}{17 \times Q} \times 100\% \quad (2)$$

where c_{NH3} (μg mL^{-1}) is the measured NH_3 concentration, V (mL) is the volume of the electrolyte, t (h) is the reduction time, A (cm^{-2}) is the surface area of CC (1 × 1 cm^2), F (96500 C mol^{-1}) is the Faraday constant, Q (C) is the quantity of applied electricity.

Characterizations

X-ray diffraction (XRD) pattern was collected on a Rigaku D/max 2400 diffractometer. X-ray photoelectron spectroscopy (XPS) analysis was conducted on a PHI 5702 spectrometer. Transmission electron microscopy (TEM) and high-resolution transmission electron microscopy (HRTEM) were recorded on a Tecnai G2 F20 microscope. Spherical aberration-corrected scanning transmission electron microscopy (AC-STEM) was performed on a Titan Cubed Themis G^2 300 microscope. Online differential electrochemical mass spectrometry (DEMS, QAS 100) was performed by QAS 100 spectrometer. Various products during the electrolysis reactions were monitored at different values of m/z ionic signals.

Calculation details

Cambridge sequential total energy package (CASTEP) module was employed for the density functional theory (DFT) calculations[4]. Electron-exchange correlations were represented by the functional of Perdew-Burke-Ernzerhof (PBE) of the generalized gradient approximation (GGA). The van der Waals interactions were

evaluated by employing the Grimme (DFT+D) scheme. The convergence criteria for structure optimization were set to: (1) energy tolerance of 1×10^{-5} eV, (2) maximum force tolerance of 0.02 eV $Å^{-1}$, (3) Monkhorst-Pack k-point sampling: 2 × 2 × 1. The cutoff energy for the plane wave basis was set at 420 eV. Monoclinic ZrO_2 (-111) was modeled by a 3 × 3 supercell, and a vacuum region of 15 Å was used to separate adjacent slabs.

The free energies (ΔG, 298 K) for each reaction were given after correction[5]:

$$\Delta G = \Delta E + \Delta ZPE - T\Delta S \quad (3)$$

where ΔE is the adsorption energy, ΔZPE is the zero-point energy difference and TΔS is the entropy difference between the gas phase and adsorbed state.

The Forcite module was employed for the MD simulations[6]. The electrolyte system was modeled by a cubic cell with placing catalyst at the center of the cell and randomly filling 1000 H_2O, 50 NO molecules, and 50 H atoms. The force field type was chosen as universal. After geometry optimization, the MD simulations were carried out with the total simulation time of 1 ns at a time step of 1 fs. The radial distribution function (RDF) is calculated by[7]:

$$g(r) = \frac{dN}{4\pi\rho r^2 dr} \quad (4)$$

where dN is the amount of NO_2^- in the shell between the central particle r and $r+dr$, ρ is the number density of NO_2^- and H.

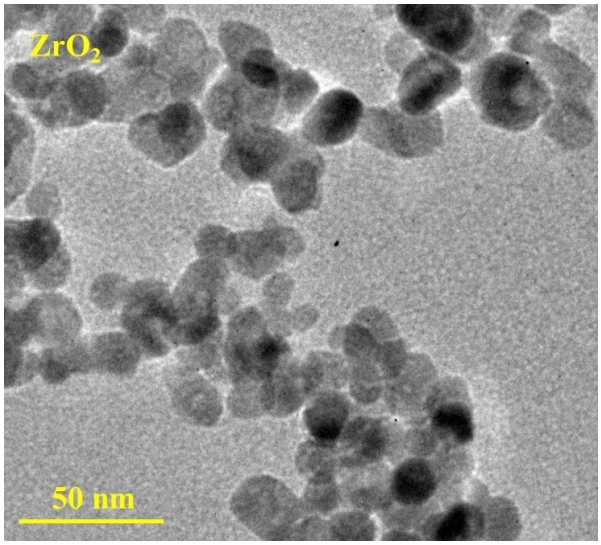

Figure S1. TEM image of ZrO_2.

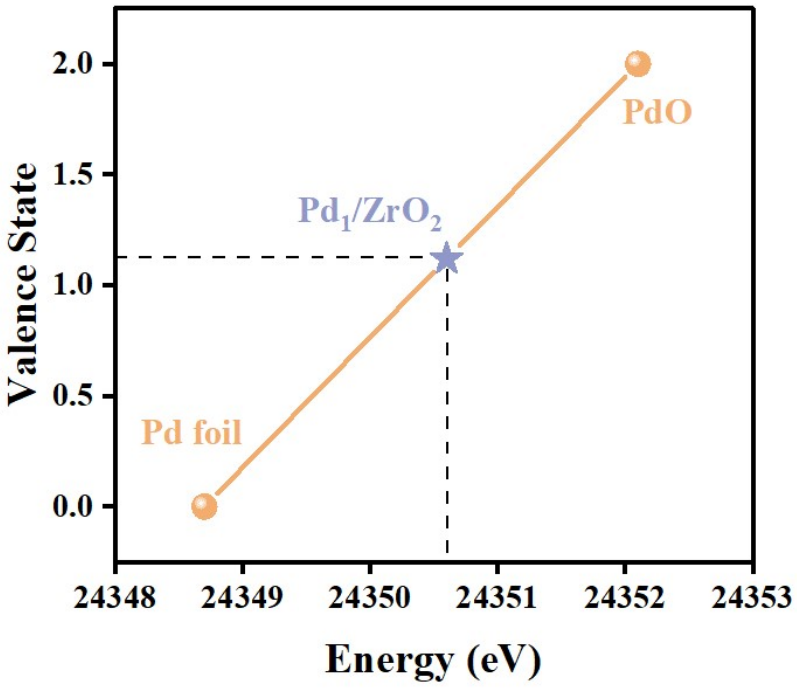

Figure S2. XANES fitted curve to determine the average Pd valence state of Pd_1/ZrO_2.

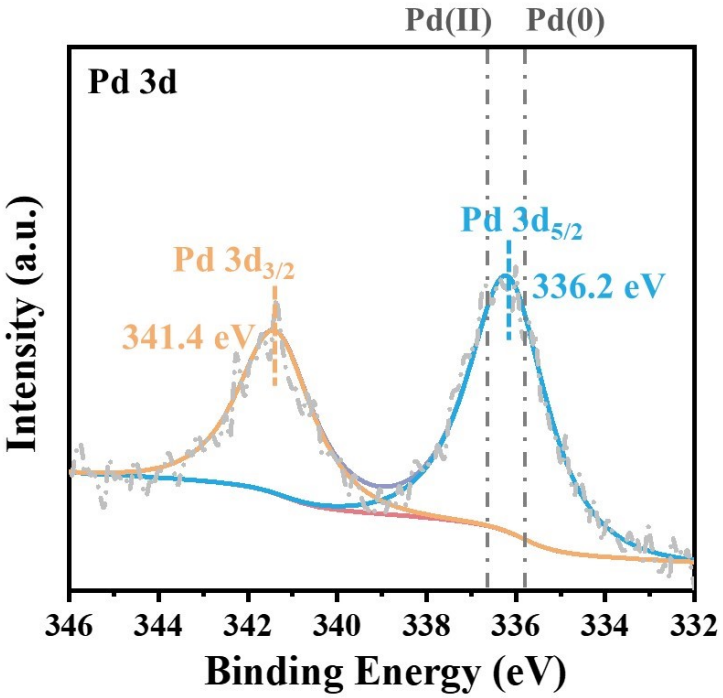

Figure S3. XPS Pd 3d spectra of Pd_1/ZrO_2.

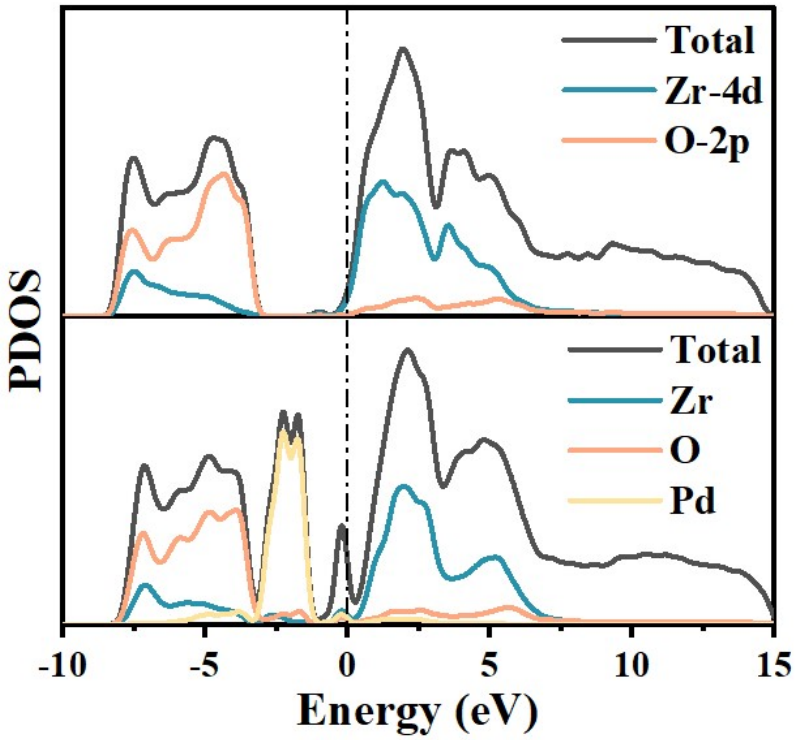

Figure S4. PDOS profiles of ZrO_2 and Pd_1/ZrO_2.

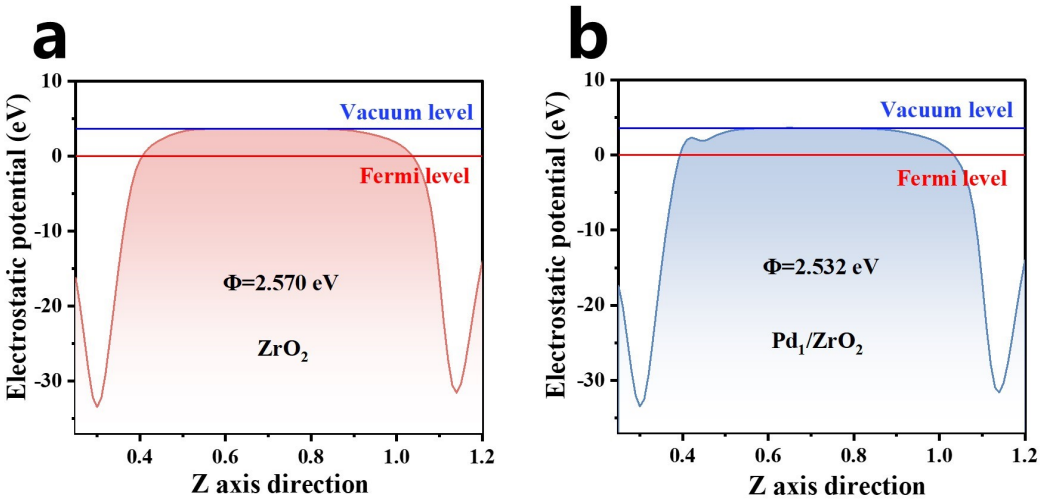

Figure S5. Average potential profiles along c-axis direction for calculating the work functions (Φ) of (a) ZrO_2 and (b) Pd_1/ZrO_2.

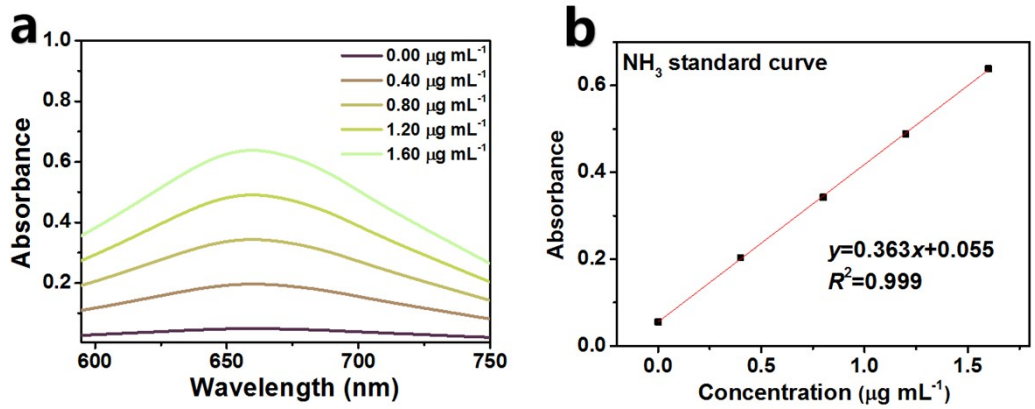

Figure S6. UV-vis absorption spectra of NH_4^+ assays after incubated for 2 h at ambient conditions. (b) Calibration curve used for the calculation of NH_3 concentrations.

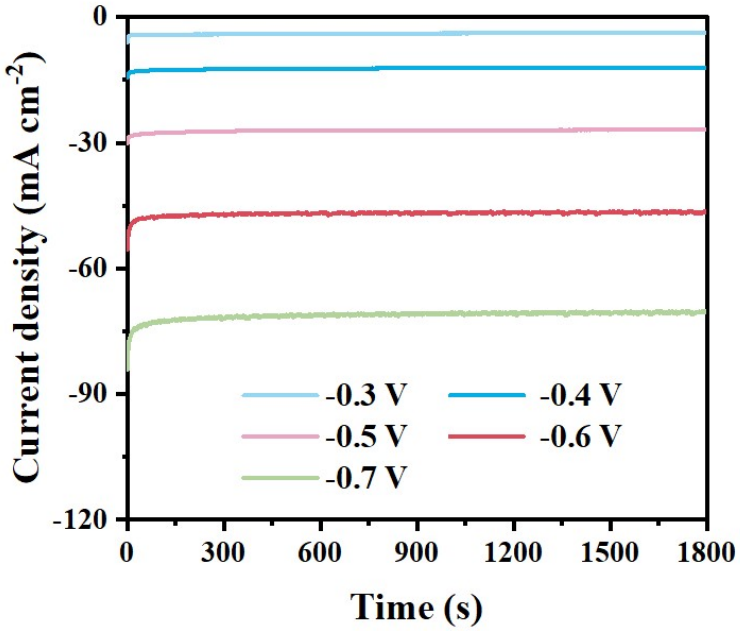

Figure S7. Chronoamperometry test of ZrO_2 in H cell.

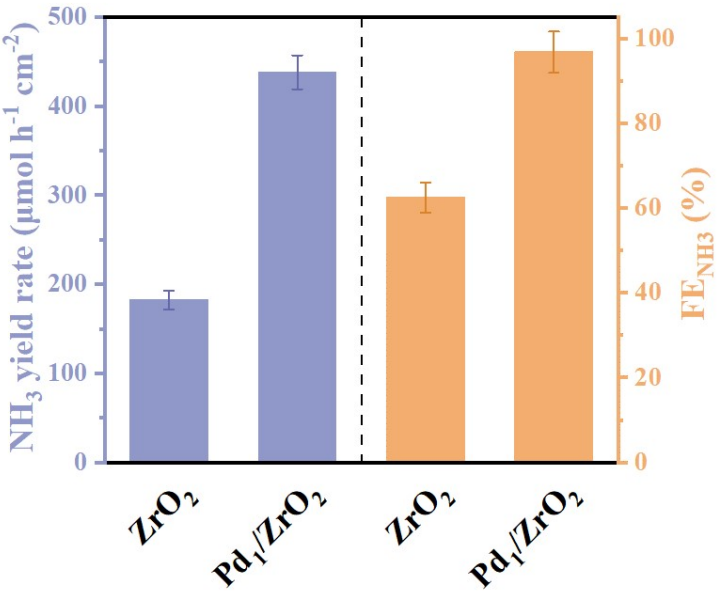

Figure S8. Comparison of NO_2RR performance between ZrO_2 and Pd_1/ZrO_2.

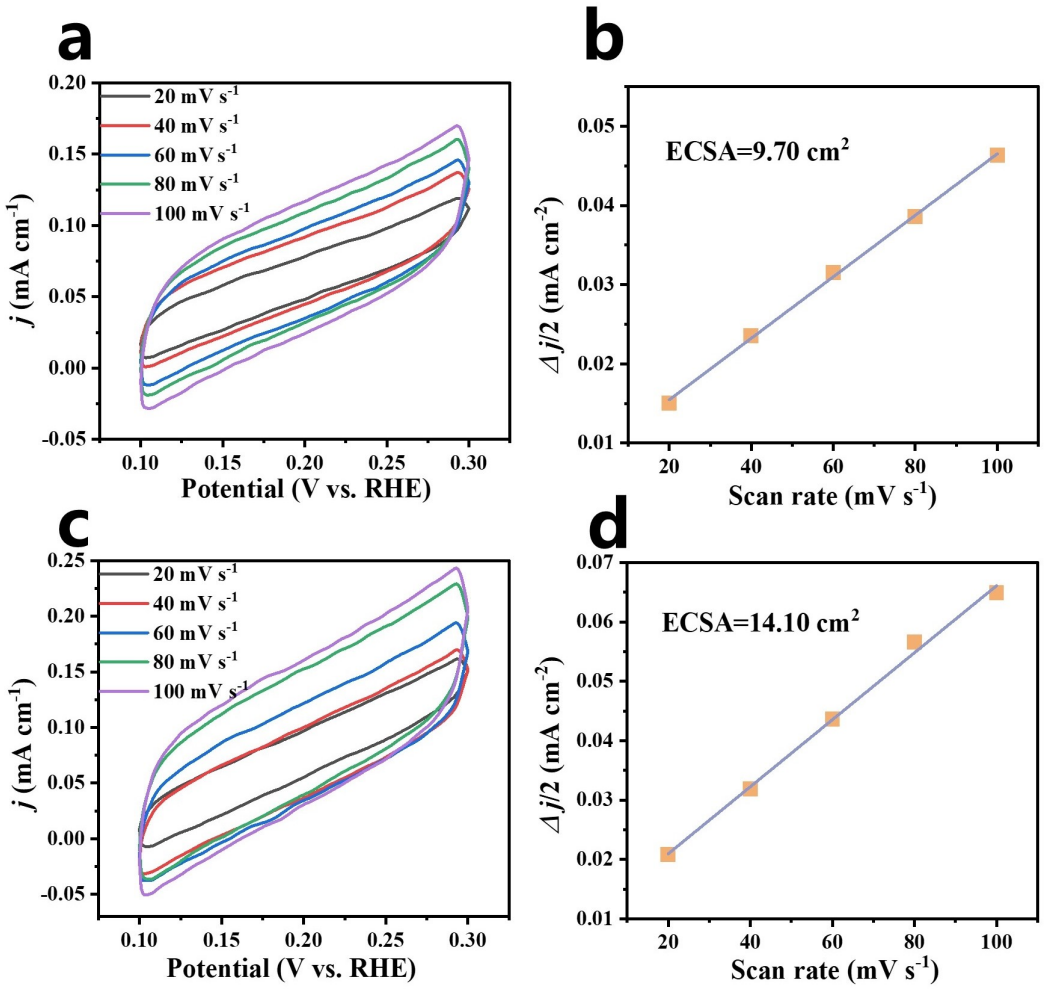

Figure S9. CV measurements at different scanning rates and calculated electrochemically active surface area (ECSA) for (a, b) ZrO_2, (c, d) Pd_1/ZrO_2.

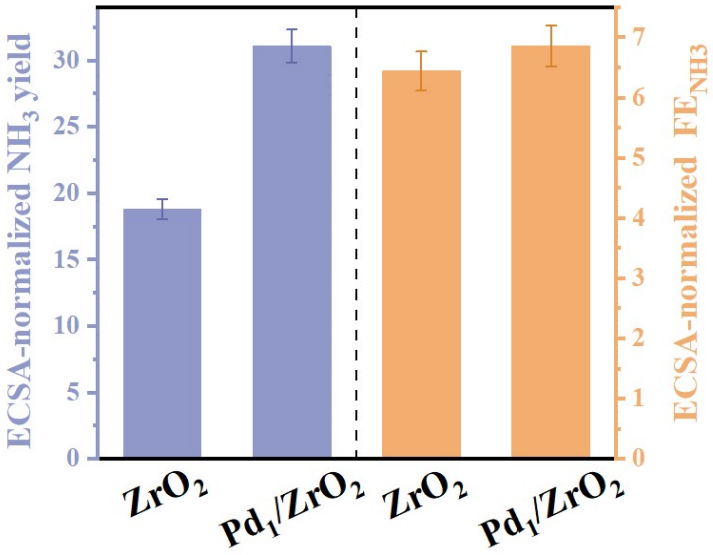

Figure S10. ECSA-normalized NH_3 yield rate and FE_{NH3} of ZrO_2 and Pd_1/ZrO_2 at -0.6 V.

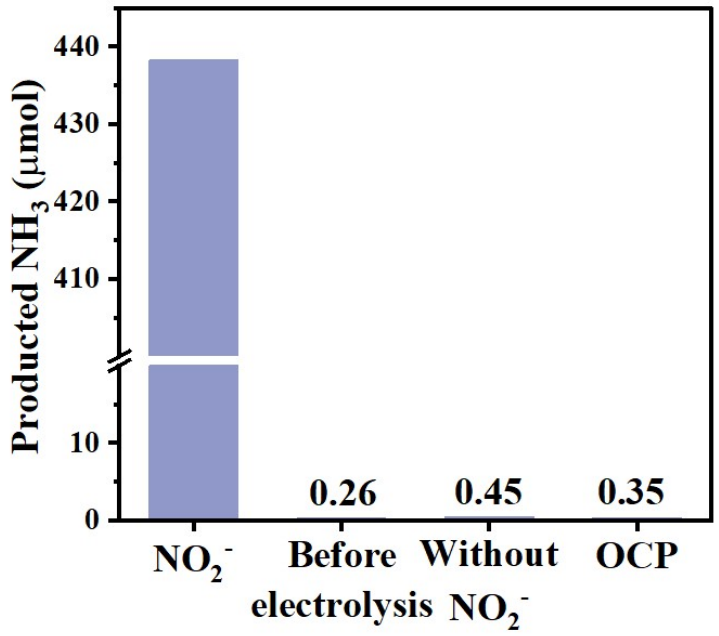

Figure S11. Amounts of produced NH_3 on Pd_1/ZrO_2 under different conditions: (1) electrolysis in NO_2^--containing solution at -0.6 V, (2) before electrolysis, (3) electrolysis in NO_2^--free solution at -0.6 V; (4) electrolysis in NO_2^--containing solution at open-circuit potential (OCP).

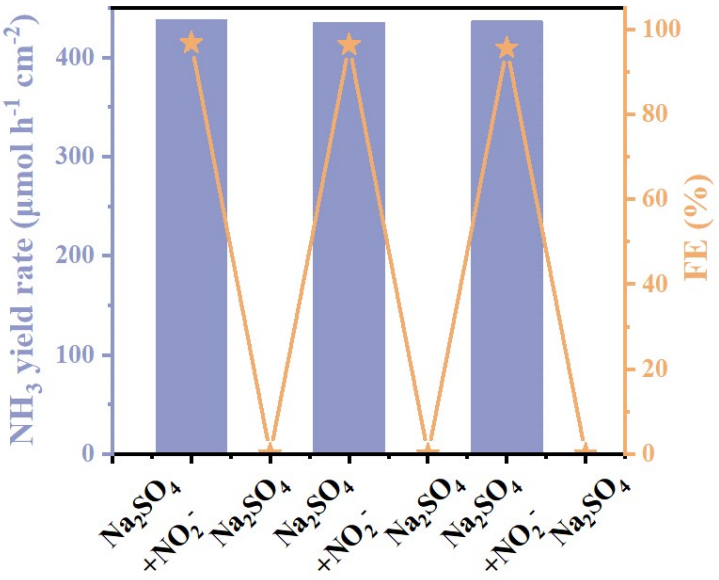

Figure S12. Alternating cycling test on Pd_1/ZrO_2 with/without NO_2^- at -0.6 V.

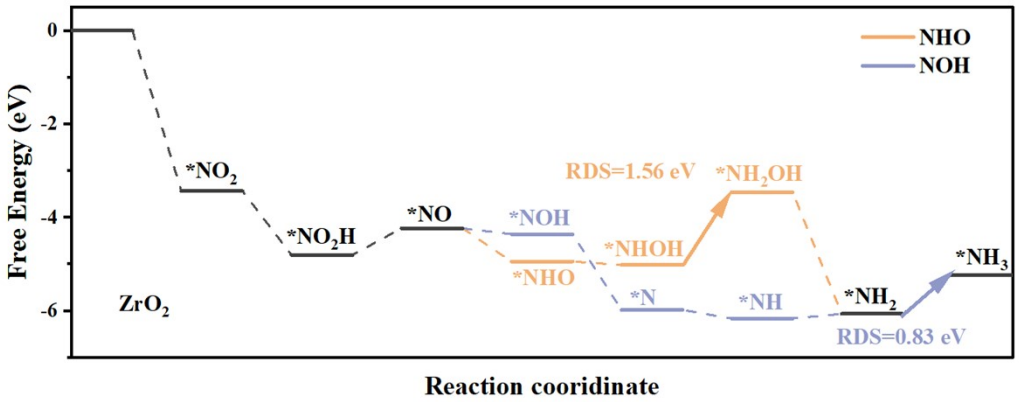

Figure S13. Free energy diagrams of various NO_2RR pathways (NHO/NOH) on ZrO_2.

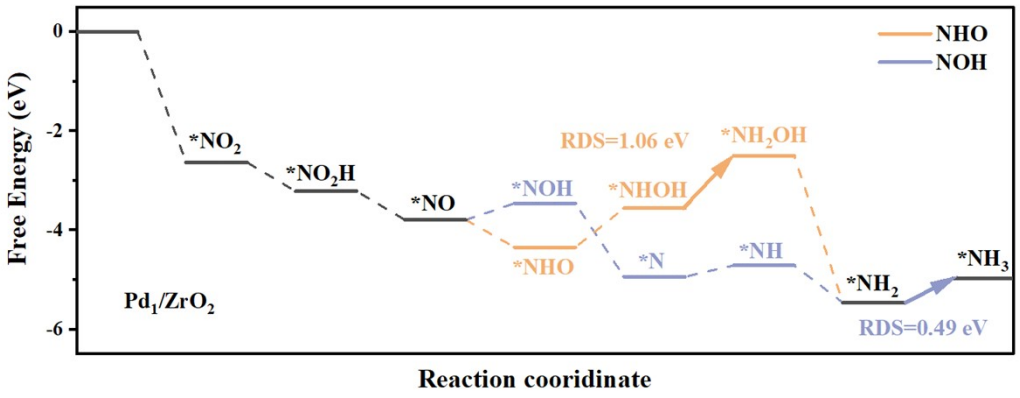

Figure S14. Free energy diagrams of various NO_2RR pathways (NHO/NOH) on Pd_1/ZrO_2.

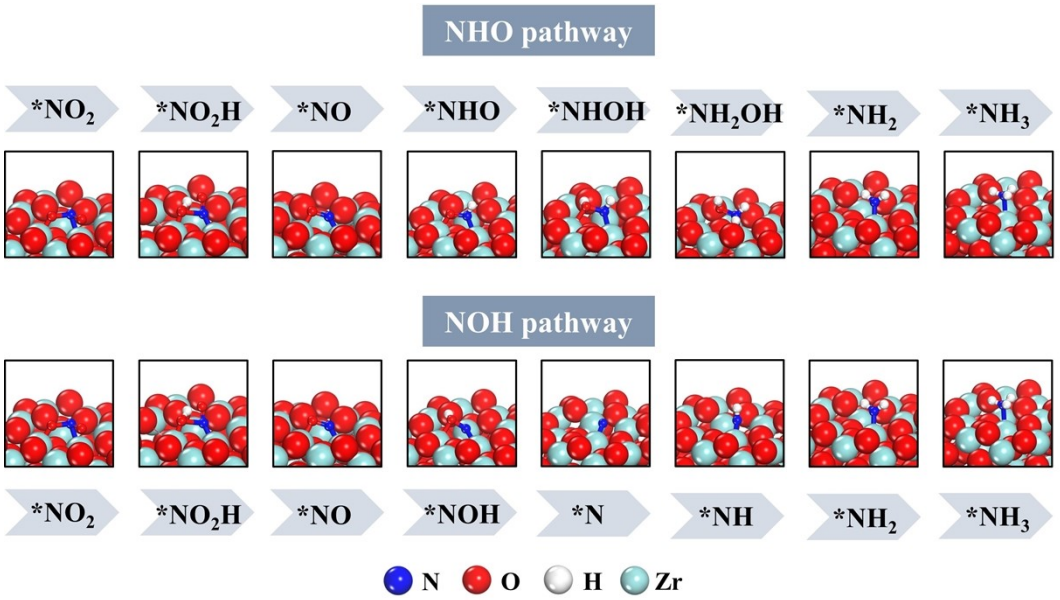

Figure S15. Optimized structures of the reaction intermediates involved in NHO/NOH pathways on ZrO_2.

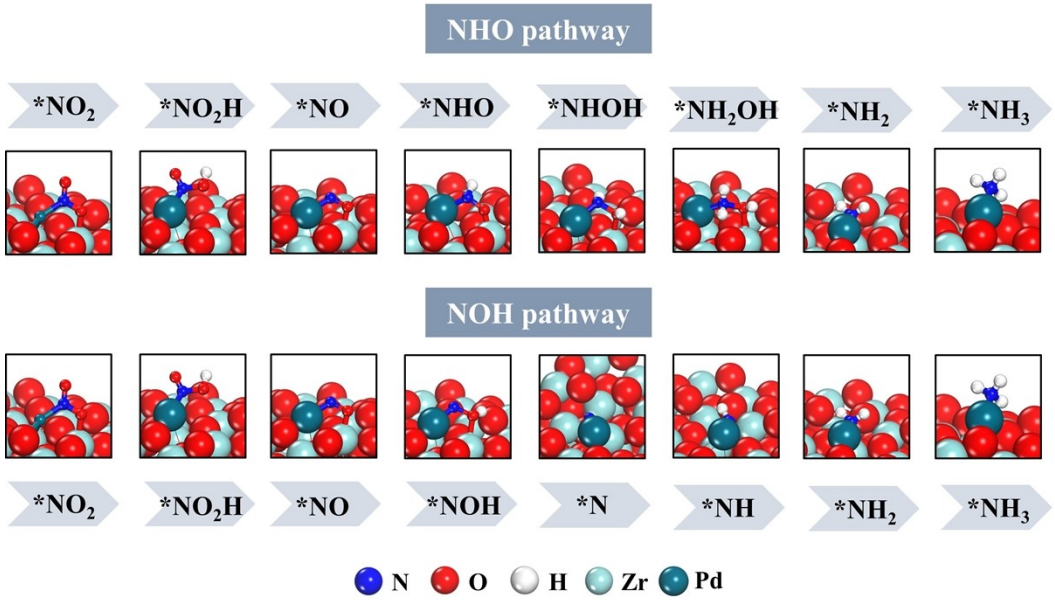

Figure S16. Optimized structures of the reaction intermediates involved in NHO/NOH pathways on Pd_1/ZrO_2.

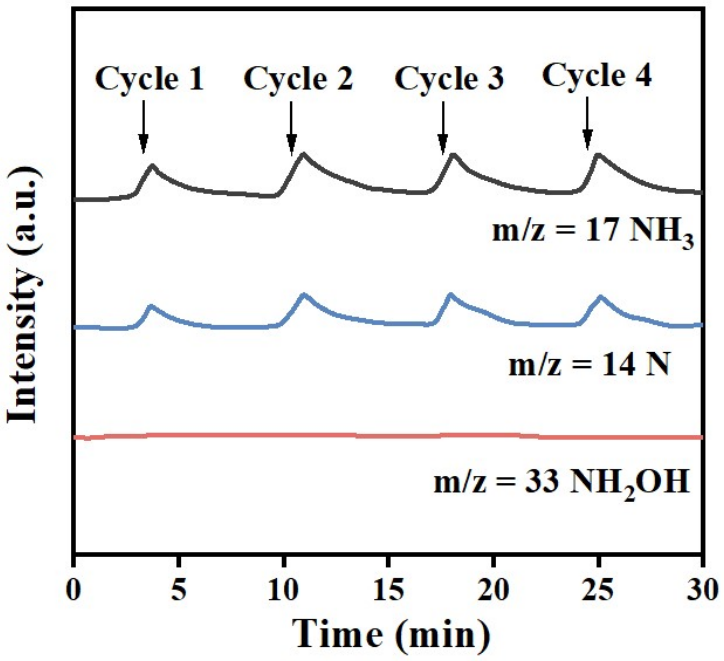

Figure S17. Online DEMS spectra of ZrO_2 during NO_2RR electrolysis at -0.6 V.

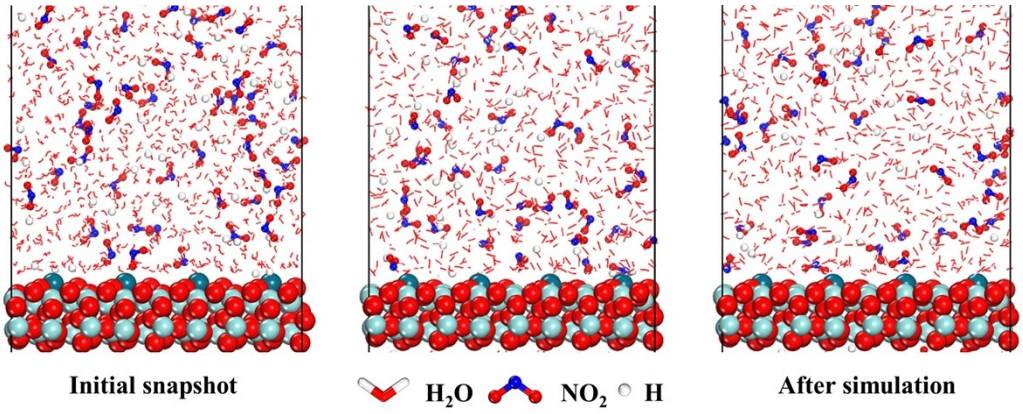

Figure S18. *NO_2/*H snapshots of Pd_1/ZrO_2 before and after simulation.

Table S1. Pd K-edge EXAFS fitting results of Pd_1/ZrO_2.

Sample	Shell	CN	R (Å)	σ^2 (10^{-3}Å)	$\lvert\Delta E_0\rvert$ (eV)	R factor
Pd_1/ZrO_2	Pd-O	1.25	2.01	6.1	4.9	0.12
	Pd-Zr	1.17	2.78			

CN is the coordination number, R is interatomic distance, σ^2 is Debye-Waller factor, ΔE_0 is edge-energy shift, R factor is used to value the goodness of the fitting.

Table S2. Comparison of the optimum NH_3 yield and FE_{NH3} for the recently reported state of the art NO_2RR electrocatalysts at ambient conditions.

Catalyst	**Electrolyte**	**NH_3 yield rate ($\mu mol\ h^{-1}\ cm^{-2}$)**	**FE_{NH3} (%)**	**Potential (V vs RHE)**	**Ref**
P-TiO_2/TP	0.1 M Na_2SO_4 (0.1 M NO_2^-)	560.8	90.6	-0.6 V	8
Cu_3P NA/CF	0.1 M PBS (0.1 M $NaNO_2$)	95.7±2.1	91.2±2.5	-0.5 V	9
Ag@NiO/CC	0.1 M NaOH (0.1 M NaO_2)	338.3	96.1	-0.7 V	10
CoP NA/TM	0.1 M PBS (500 ppm NO_2^-)	132.7±3.0	90.0±2.3	-0.2 V	11
ITO@TiO_2/TP	0.5 M $LiClO_4$ (0.1 M NO_2)	411.3	82.6	-0.5 V	12
Pd/CuO NOs	0.1 M K_2SO_4 (0.01 M KNO_2)	53.3	91.8	-1.5 V	13
Ni@MDC	0.1 M NaOH (0.1 M NO_2^-)	300	65.4	-0.8 V	14
CF@Cu_2O	0.1 M PBS (0.1 M $NaNO_2$)	441.8	94.2	-0.6 V	15
Ni-TiO_2/TP	0.1 M NaOH (0.1 M NO_2^-)	380.27	94.89	-0.5 V	16
Pd_1/ZrO_2	**0.1 M Na_2SO_4 (0. 1 M NO_2^-)**	**438.06**	**96.75**	**-0.6 V**	**This Work**

References

1. D. Zhu, L. Zhang, R. E. Ruther and R. J. Hamers, Photo-illuminated diamond as a solid-state source of solvated electrons in water for nitrogen reduction, *Nat. Mater.*, 2013, **12**, 836.
2. G. W. WATT and J. D. CHRISP, A spectrophotometric method for the determination of hydrazine, *Anal. Chem.*, 1952, **24**, 2006-2008.
3. P. Li, Z. Jin, Z. Fang and G. Yu, A single-site iron catalyst with preoccupied active centers that achieves selective ammonia electrosynthesis from nitrate, *Energy Environ. Sci.*, 2021, **14**, 3522-3531.
4. S. J. Clark*, M. D. SegallII, C. J. PickardII, P. J. HasnipIII, M. I. J. ProbertIV, K. RefsonV and M. C. PayneII, First principles methods using CASTEP, *Z. Kristallogr.-Cryst. Mater.*, 2005, **220**, 567–570.
5. J. Wang, J. Liang, P. Liu, Z. Yan, L. Cui, L. Yue, L. Zhang, Y. Ren, T. Li, Y. Luo, Q. Liu, X.-E. Zhao, N. Li, B. Tang, Y. Liu, S. Gao, A. M. Asiri, H. Hao, R. Gao and X. Sun, Biomass Juncus derived carbon decorated with cobalt nanoparticles enables high-efficiency ammonia electrosynthesis by nitrite reduction, *J. Mater. Chem. A*, 2022, **10**, 2842-2848.
6. K. Chu, Y. Luo, P. Shen, X. Li, Q. Li and Y. Guo, Unveiling the synergy of O-vacancy and heterostructure over MoO_{3-x}/MXene for N_2 electroreduction to NH_3, *Adv. Energy Mater.*, 2021, **12**, 2103022.
7. X. Li, P. Shen, X. Li, D. Ma and K. Chu, Sub-nm RuO_x clusters on Pd metallene for synergistically enhanced nitrate electroreduction to ammonia, *ACS Nano*, 2023, **17**, 1081-1090.
8. L. Ouyang, X. He, S. Sun, Y. Luo, D. Zheng, J. Chen, Y. Li, Y. Lin, Q. Liu, A. M. Asiri and X. Sun, Enhanced electrocatalytic nitrite reduction to ammonia over P-doped TiO_2 nanobelt array, *J. Mater. Chem. A*, 2022, **10**, 23494-23498.
9. J. Liang, B. Deng, Q. Liu, G. Wen, Q. Liu, T. Li, Y. Luo, A. A. Alshehri, K. A. Alzahrani, D. Ma and X. Sun, High-efficiency electrochemical nitrite reduction to ammonium using a Cu_3P nanowire array under ambient conditions, *Green Chem.*, 2021, **23**, 5487-5493.
10. Q. Liu, G. Wen, D. Zhao, L. Xie, S. Sun, L. Zhang, Y. Luo, A. Ali Alshehri, M. S. Hamdy, Q. Kong and X. Sun, Nitrite reduction over Ag nanoarray electrocatalyst for ammonia synthesis, *J. Colloid Interface Sci.*, 2022, **623**, 513-519.
11. G. Wen, J. Liang, Q. Liu, T. Li, X. An, F. Zhang, A. A. Alshehri, K. A. Alzahrani, Y. Luo, Q. Kong and X. Sun, Ambient ammonia production via electrocatalytic nitrite reduction catalyzed by a CoP nanoarray, *Nano Res.*, 2022, **15**, 972-977.
12. S. Li, J. Liang, P. Wei, Q. Liu, L. Xie, Y. Luo and X. Sun, ITO@TiO_2 nanoarray: An efficient and robust nitrite reduction reaction electrocatalyst toward NH_3 production under ambient conditions, *eScience*, 2022, **2**, 382-388.
13. S. Liu, L. Cui, S. Yin, H. Ren, Z. Wang, Y. Xu, X. Li, L. Wang and H. Wang, Heterointerface-triggered electronic structure reformation: Pd/CuO nano-olives motivate nitrite electroreduction to ammonia, *Appl. Catal. B*, 2022, **319**, 121876.
14. X. He, X. Li, X. Fan, J. Li, D. Zhao, L. Zhang, S. Sun, Y. Luo, D. Zheng, L. Xie, A. M. Asiri, Q. Liu and X. Sun, Ambient electroreduction of nitrite to ammonia over Ni nanoparticle supported on molasses-derived carbon sheets, *ACS Appl. Nano Mater.*, 2022, **5**, 14246-14250.
15. Q. Chen, X. An, Q. Liu, X. Wu, L. Xie, J. Zhang, W. Yao, M. S. Hamdy, Q. Kong and X. Sun, Boosting electrochemical nitrite–ammonia conversion properties by a Cu foam@Cu_2O catalyst, *Chem. Commun.*, 2022, **58**, 517-520.

16. Z. Cai, C. Ma, D. Zhao, X. Fan, R. Li, L. Zhang, J. Li, X. He, Y. Luo, D. Zheng, Y. Wang, B. Ying, S. Sun, J. Xu, Q. Lu and X. Sun, Ni doping enabled improvement in electrocatalytic nitrite-to-ammonia conversion over TiO_2 nanoribbon, *Mater. Today Energy*, 2023, **31**, 101220.